Supporting Information

A General Strategy to In Situ Construct $CoSe_2$-MSe_x@GA (M=Zn, Ni, Fe) Heterostructures for Effective Sodium Storage

Zhengzheng Xu,[a] Yanjiao Li,[a] Shiqi Li,[a] Yingying Chen,*[ab] Majid Farahmandjou,[b] Guoxiu Wang,[b] Hongxun Yang,*[a] and Hao Tian*[b]

[a] School of Environmental and Chemical Engineering, Jiangsu University of Science and Technology, Zhenjiang 212003, Jiangsu, China

[b] Centre for Clean Energy Technology, School of Mathematical and Physical Sciences, Faculty of Science, University of Technology Sydney, Broadway, NSW 2007, Australia.

*Corresponding author.

Email: scyyh@just.edu.cn (Y. Chen); yhongxun@126.com (H. Yang); hao.tian@uts.edu.au (H. Tian)

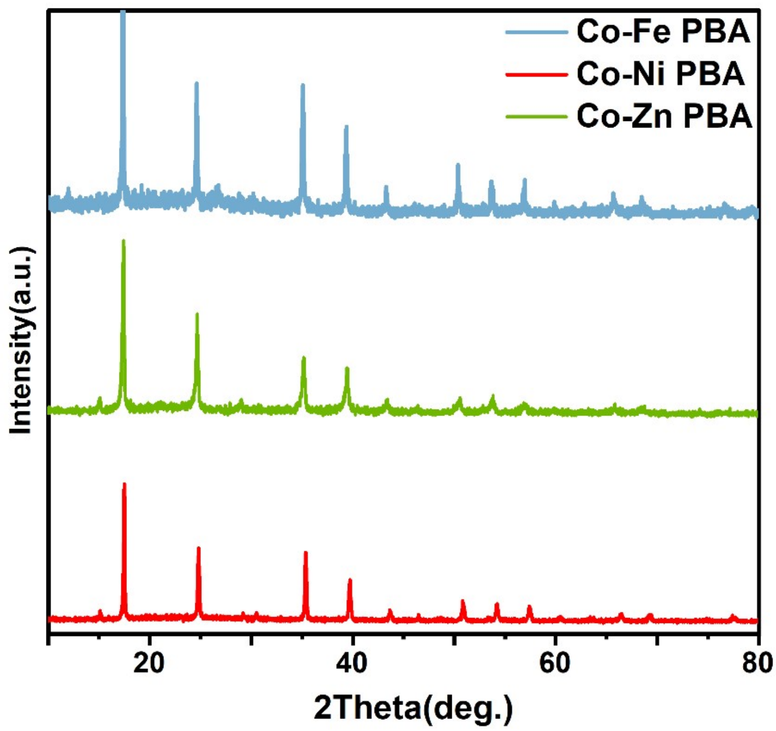

Figure S1. XRD patterns of prussian blue analog precursors.

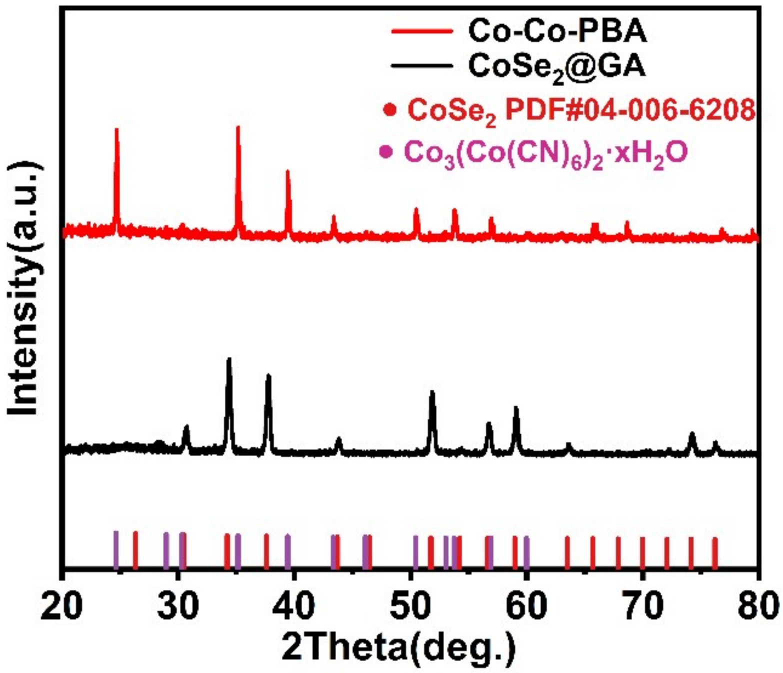

Figure S2. XRD patterns of $CoSe_2$@GA.

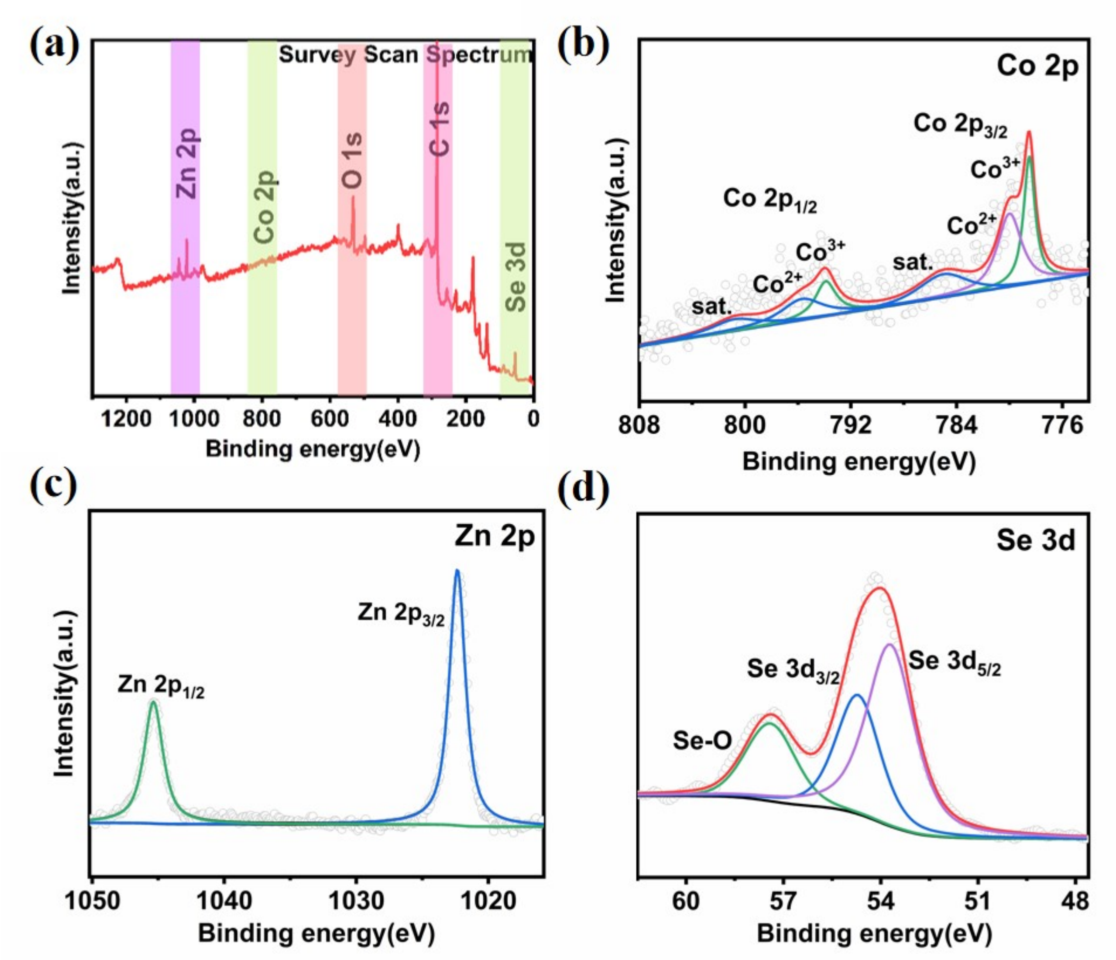

Figure S3. (a) XPS survey, (b) Co 2p, (c) Zn 2p and (d) Se 3d spectra of $CoSe_2$-ZnSe@GA.

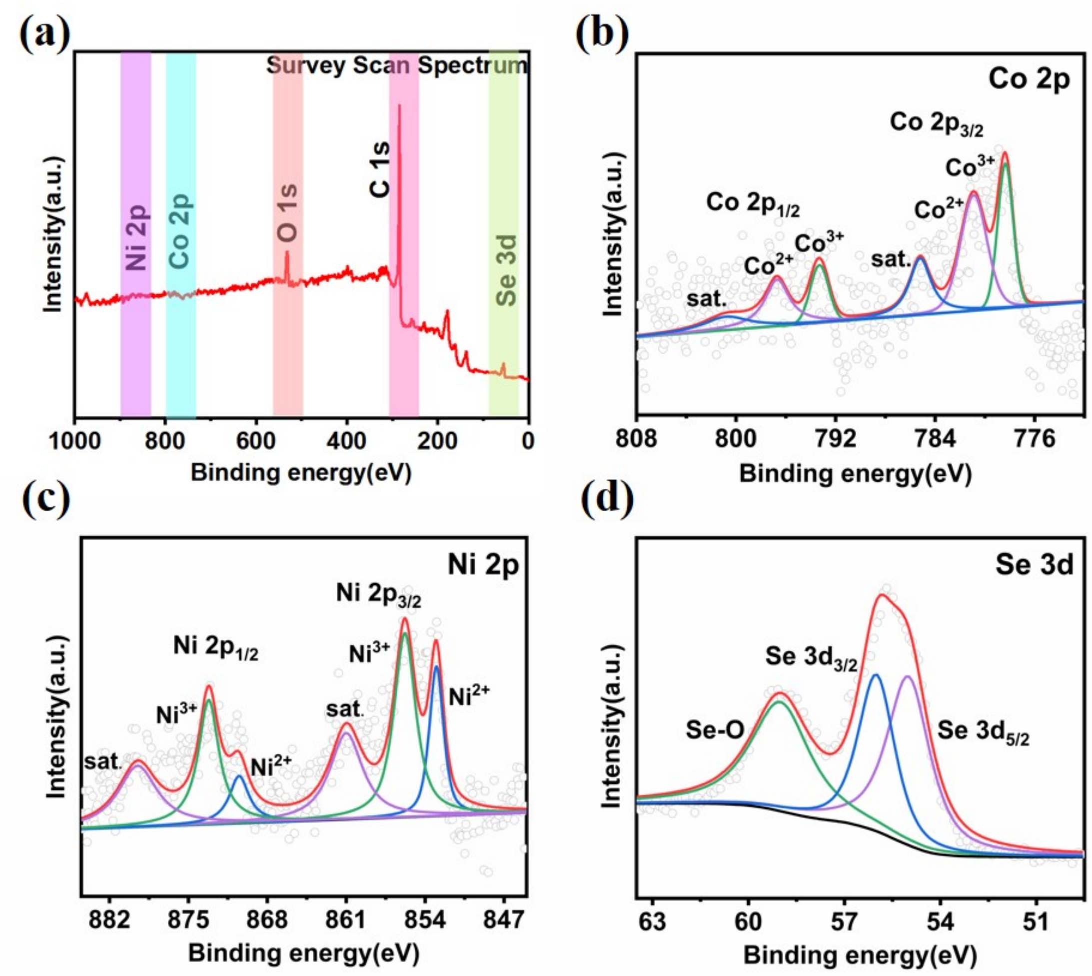

Figure S4. (a) XPS survey, (b) Co 2p, (c) Ni 2p and (d) Se 3d spectra of $CoSe_2$-$NiSe_2$@GA.

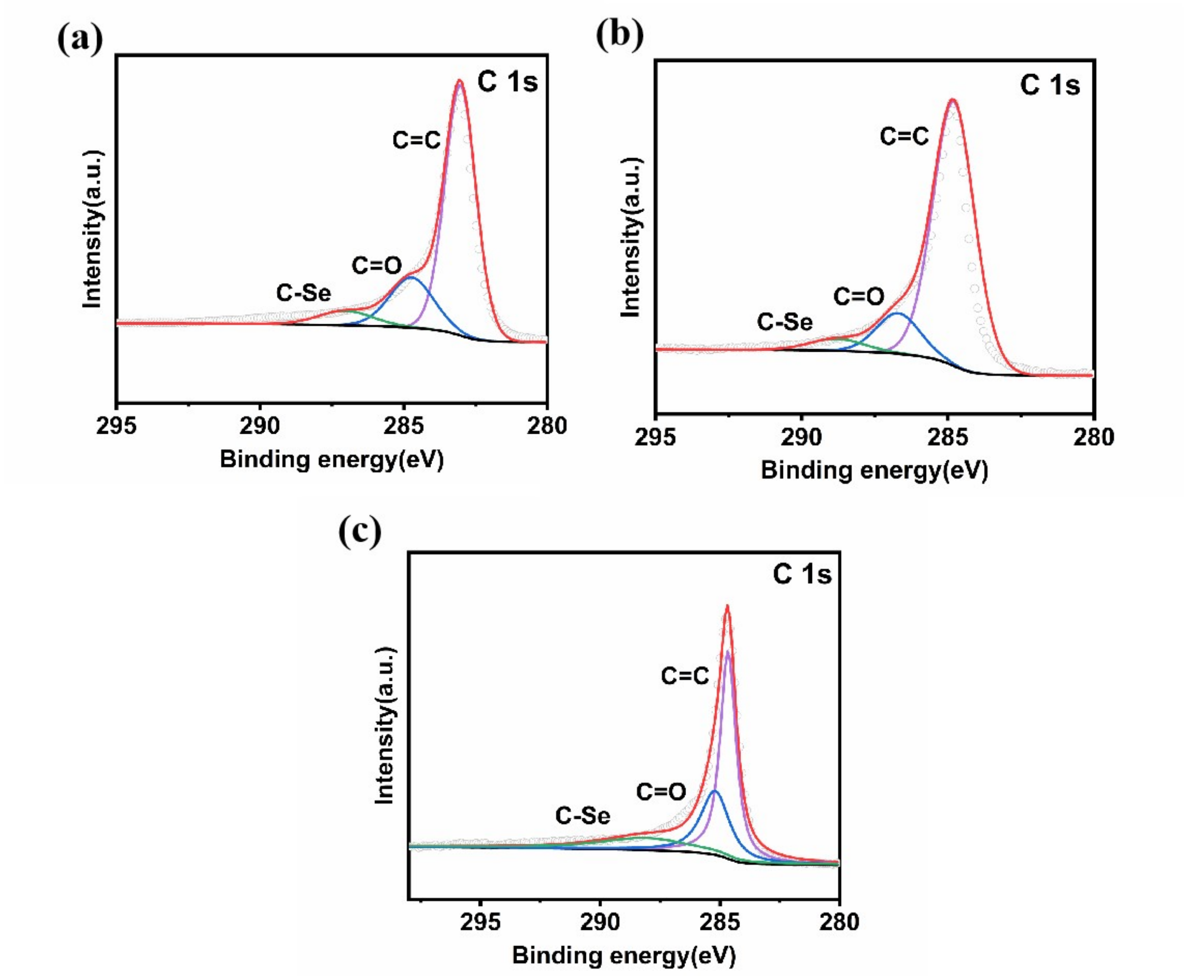

Figure S5. C 1s high resolution XPS of (a) $CoSe_2$-FeSe@GA, (b) $CoSe_2$-ZnSe@GA and (c) $CoSe_2$-$NiSe_2$@GA.

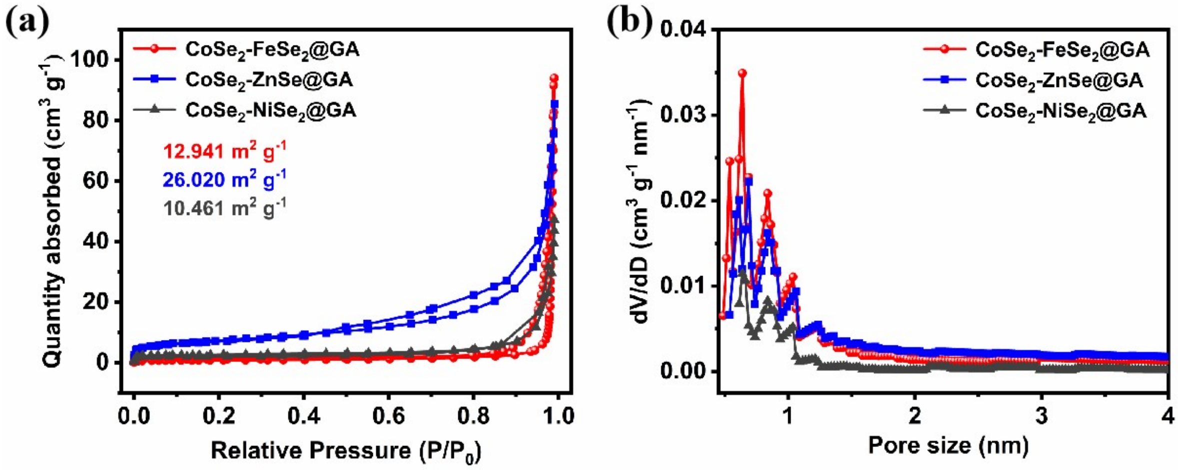

Figure S6. N_2 adsorption-desorption isotherms and pore size distribution plots of $CoSe_2$-$FeSe_2$@GA, $CoSe_2$-ZnSe@GA, and $CoSe_2$-$NiSe_2$@GA.

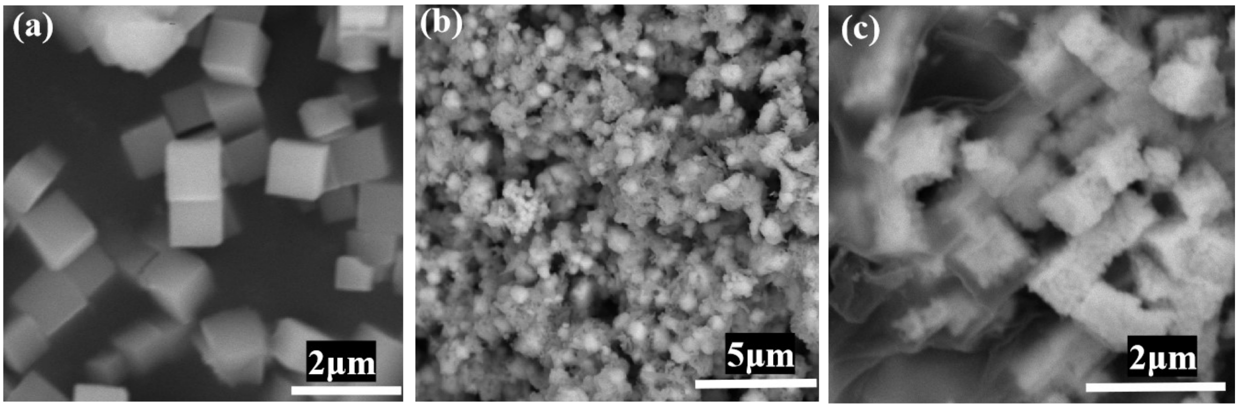

Figure S7. SEM images of (a) Co-Co-PBAs, (b) $CoSe_2$ and (c) $CoSe_2$@GA.

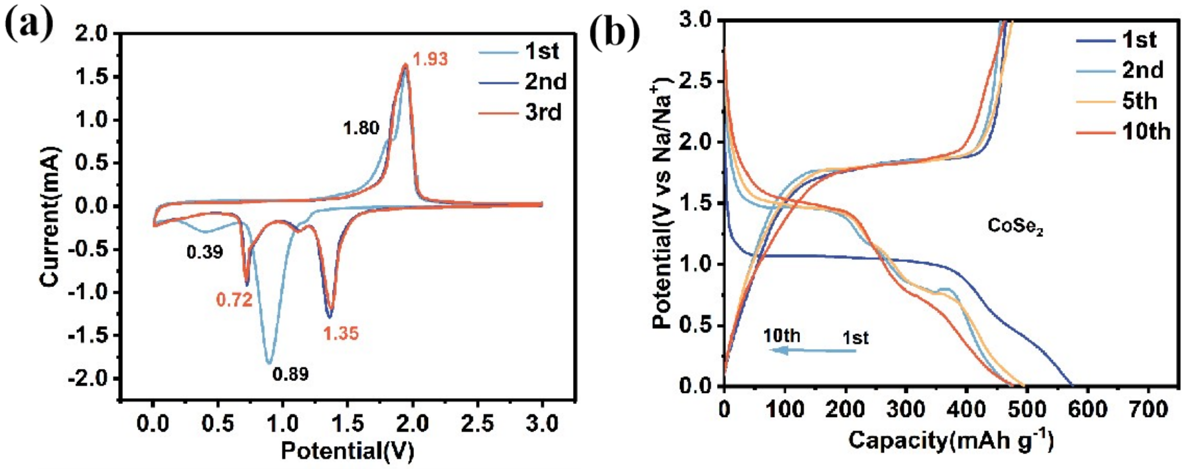

Figure S8. (a) CV curves of $CoSe_2$ at 0.2 mV s^{-1}, (b) The charge–discharge profiles of $CoSe_2$ at 0.2 A g^{-1}.

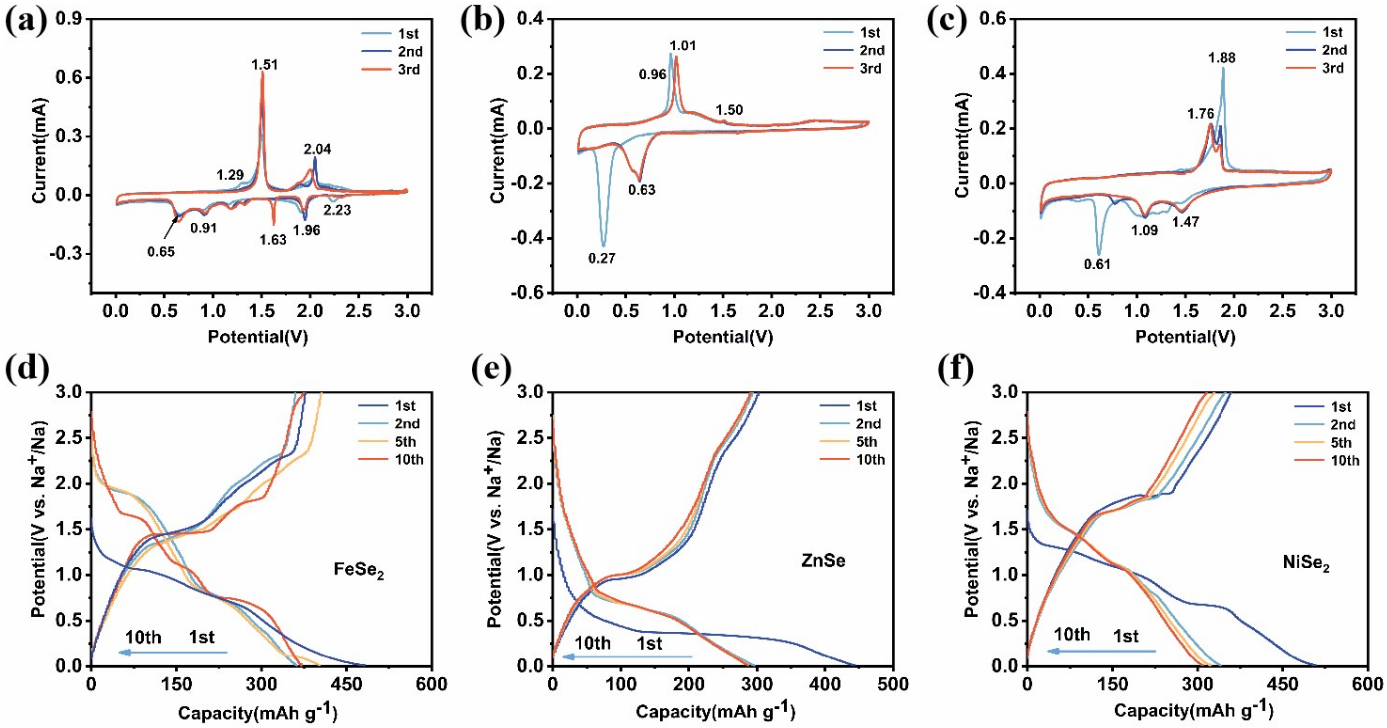

Figure S9. CV curves at 0.2 mV s^{-1} of (a) $FeSe_2$, (b) ZnSe, and (c) $NiSe_2$; The charge–discharge profiles of (a) $FeSe_2$, (b) ZnSe, and (c) $NiSe_2$ at the 1^{st}, 2^{nd}, 5^{th} and 10^{th} cycle.

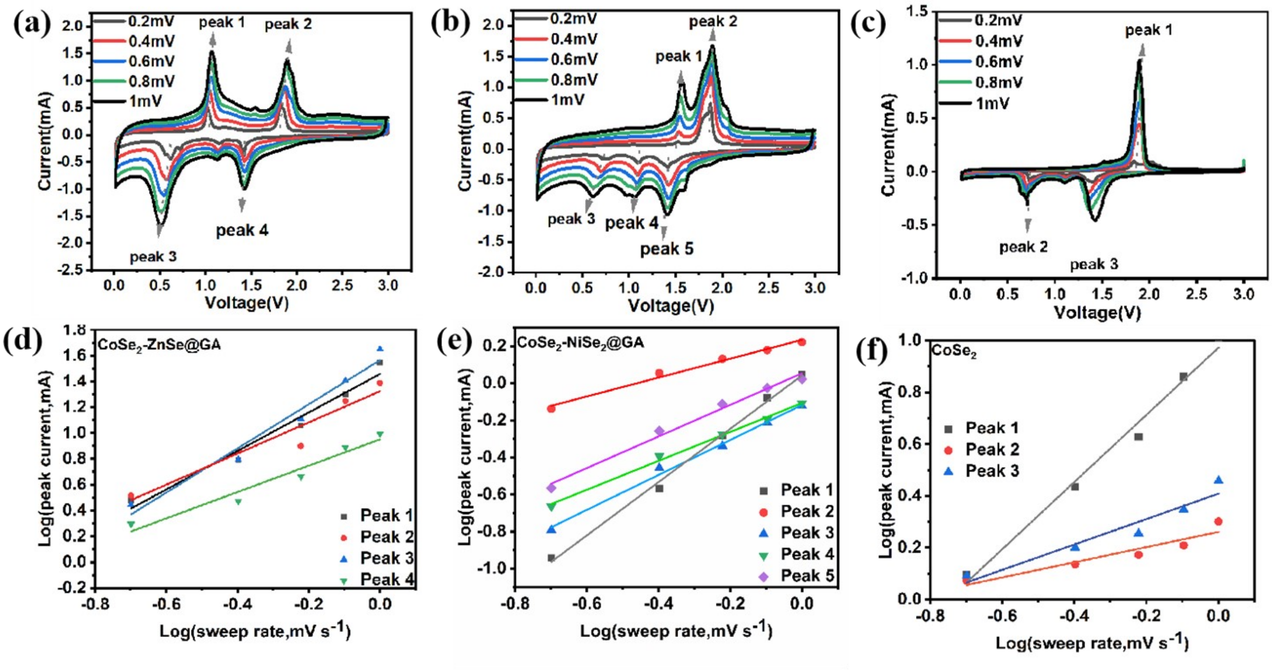

Figure S10. CV curves at different scan rates (from 0.2 to 1 mV s^{-1}) of (a) $CoSe_2$-ZnSe@GA, (b) $CoSe_2$-$NiSe_2$@GA, (c) $CoSe_2$. Log(i) vs log(v) plots of (d) $CoSe_2$-ZnSe@GA, (e) $CoSe_2$-$NiSe_2$@GA and (f) $CoSe_2$.

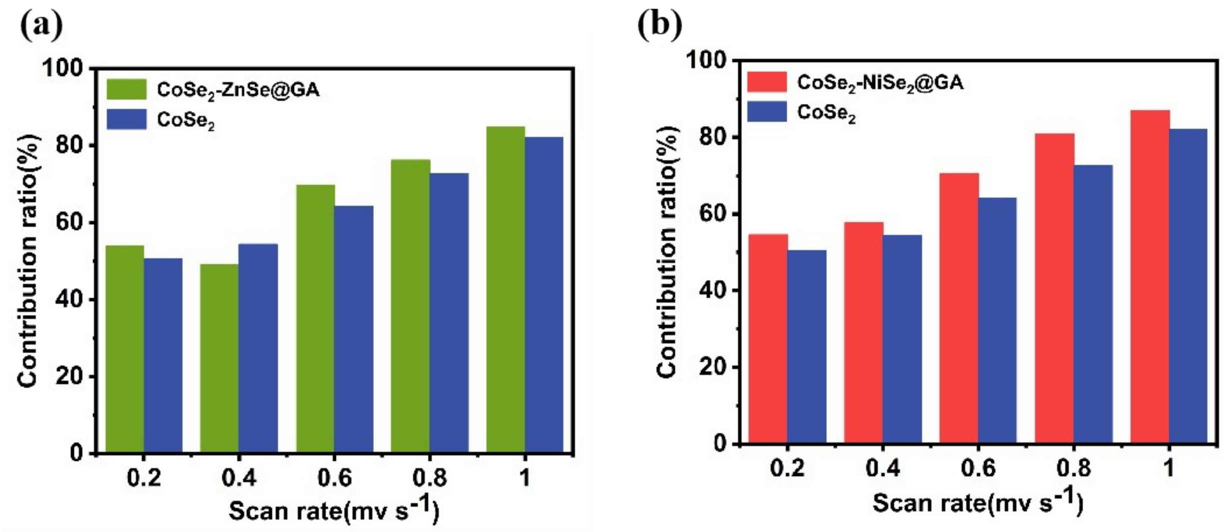

Figure S11. Pseudocapacitance contribution rate at different scan rate of (a) $CoSe_2$-ZnSe@GA and $CoSe_2$, (b) $CoSe_2$-$NiSe_2$@GA and $CoSe_2$.

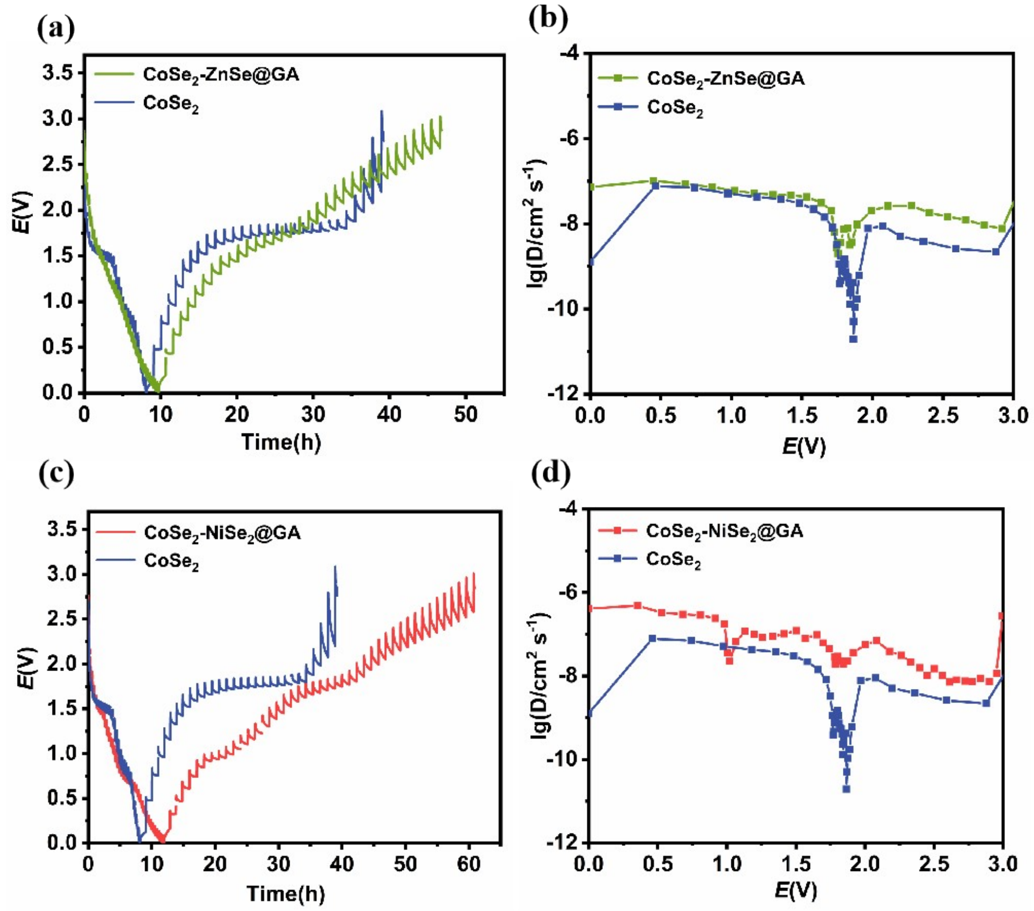

Figure S12. (a) GITT voltage curves and (b) Na^+ diffusion coefficients for $CoSe_2$-ZnSe@GA and $CoSe_2$. (c) GITT voltage curves and (d) Na^+ diffusion coefficients for $CoSe_2$-$NiSe_2$@GA and $CoSe_2$.

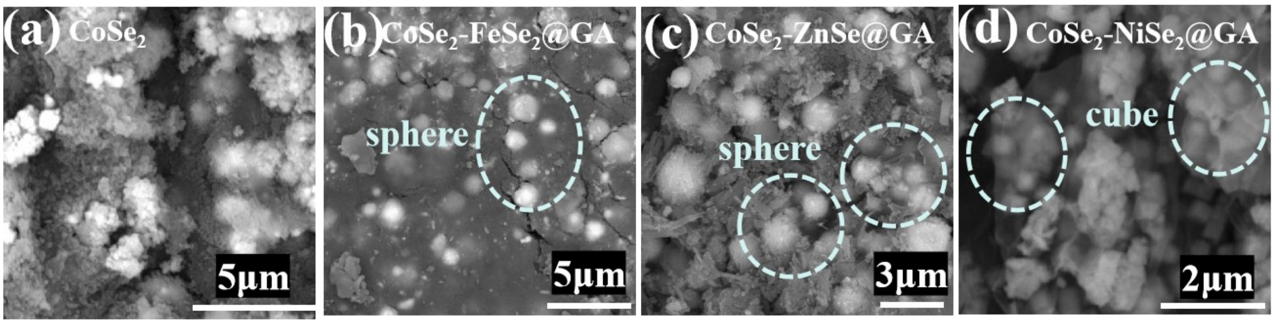

Figure S13. SEM imagines of (a) $CoSe_2$, (b) $CoSe_2$-$FeSe_2$@GA, (c) $CoSe_2$-ZnSe@GA and (d) $CoSe_2$-$NiSe_2$@GA after cycling.

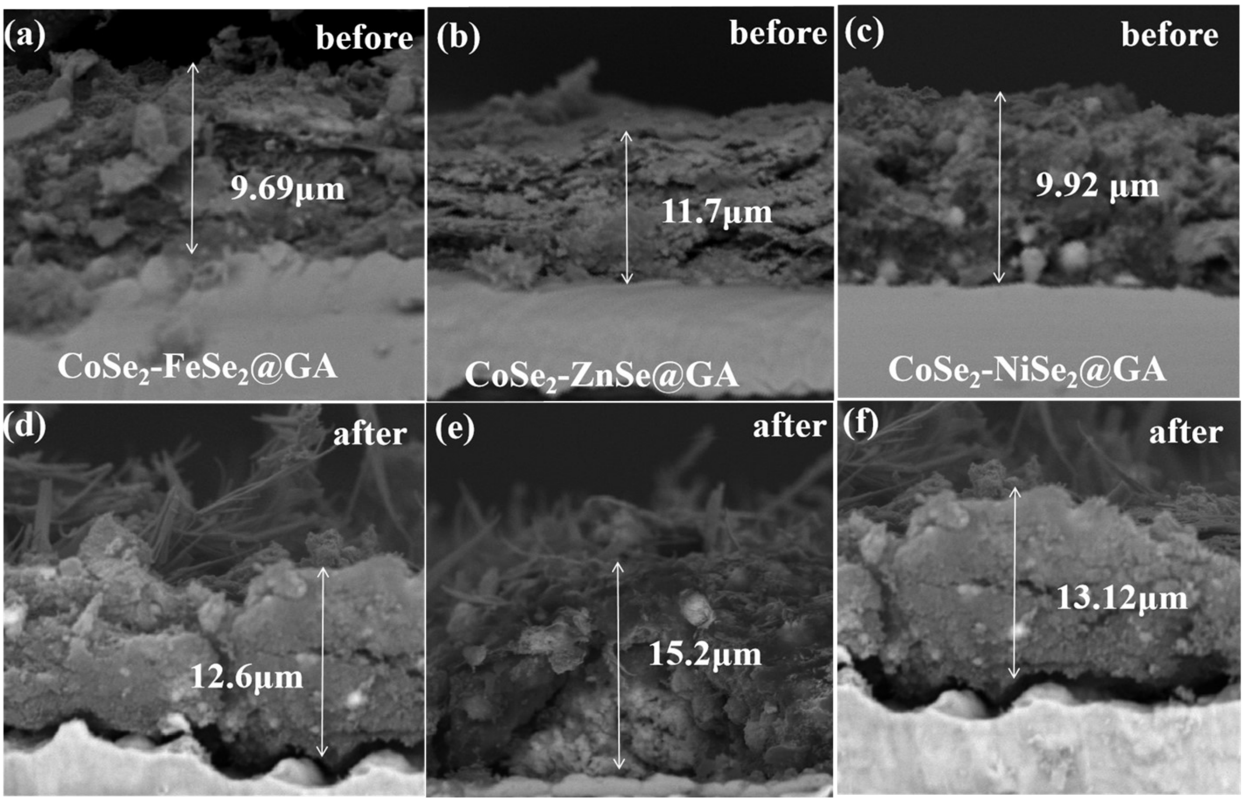

Figure S14. SEM imagines before cycling of (a) $CoSe_2$-$FeSe_2$@GA, (b) $CoSe_2$-ZnSe@GA and (c) $CoSe_2$-$NiSe_2$@GA, SEM imagines after cycling of (d) $CoSe_2$-$FeSe_2$@GA, (e) $CoSe_2$-ZnSe@GA and (f) $CoSe_2$-$NiSe_2$@GA.

Table S1. Details of comparison of specific surface area and pore characteristics of $CoSe_2$-$FeSe_2$@GA, $CoSe_2$-ZnSe@GA, and $CoSe_2$-$NiSe_2$@GA

Samples	S_{BET} (m^2g^{-1})	V_t (cm^3g^{-1})	V_{mic}(cm^3g^{-1})	Average pore diameter (nm)	V_{meso}(cm^3 g^{-1})
$CoSe_2$-$FeSe_2$@GA	12.941	0.14196	1.4196	48.27	1.2546
$CoSe_2$-ZnSe@GA	26.020	0.1235	5.9782	18.98	0.1192
$CoSe_2$-$NiSe_2$@GA	10.461	0.068927	2.4034	26.357	0.062994

S_{BET}: Specific surface area by BET method, V_t: Total pore volume, V_{mic}: Micropore volume, V_{meso}: Mesopore volume.

Table S2. Comparison of the electrochemical performance of existing bimetallic selenides reported in recent literatures.

Materials	**Current density ($A\ g^{-1}$)**	**Initial Discharge/charge Capacity ($mAh\ g^{-1}$)**	**ICE (%)**	**Reversible Capacity/Cycle number/Current density ($mAh\ g^{-1}$/cycle/$A\ g^{-1}$)**	**Refs.**
$CoSe_2$-$FeSe_2$@GA	0.2	723.0/677.4	97.95	722.8/1000/1.0	**This work**
$CoSe_2$-ZnSe@GA	0.2	637.4/532.2	83.5	649.6/1000/1.0	
$CoSe_2$-$NiSe_2$@GA	0.2	770.9/603.4	78.3	644.5/1000/1.0	
ZnSe/$CoSe_2$@NPC NTs(II)-700	0.05	454.8	109.1	318.4/4000/2.0	1
Ni_3Se_4@$CoSe_2$@C/CNTs	0.1	595/324	54.5	243/600/1.0	2
ZnSe@$CoSe_2$/NC	0.1	1071.1/820.9	76.6	293.3/1000/1.0	3
CoSe/$MoSe_2$-C	0.2	532.0/394.4	74.14	320.9/10000/2.0	4
(ZnSe@CoSe@CN)	0.1	660/559	84.6	429.6/200/1.0 397.1/400/2.0	5
$CoSe_2$/ZnSe	0.1	575/416	72.3	386.9/100/0.1	6
(CoNi)Se_2/NC	0.1	602/492.5	81.8	450.5/500/1.0	7
$FeSe_2$@$CoSe_2$/$FeSe_2$	0.1	—	93	542/100/0.2 529/1800/2	8
(Co,Fe) Se-NGC@PDA-20	0.1	618/376	59	306/200/1.0	9
$MoSe_2$-$Cu_{1.82}$Se@GA	0.2	672.4/503.9	75.6	444.8/1000/1.0	10
$CoSe_2$-SnSe@CNF	0.1	798.4/437.8	54.8	248.7/1000/1.0	11

Table S3. Comparison of typical EIS parameters of $CoSe_2$-$FeSe_2$@GA, $CoSe_2$-ZnSe@GA and $CoSe_2$-$NiSe_2$ before and after cycling.

Samples	$R_s(\Omega)$ (before cycling)	$R_{ct}(\Omega)$ (before cycling)	$R_s(\Omega)$ (after cycling)	$R_{ct}(\Omega)$ (after cycling)
$CoSe_2$-$FeSe_2$@GA	3.225	6.1	3.241	1.078
$CoSe_2$-ZnSe@GA	2.558	9.3	10.71	3.226
$CoSe_2$-$NiSe_2$@GA	3.545	4.0	3.256	12.43

Table S4. The calculated b-values of the four materials corresponding to the different peaks

	Peak 1	**Peak 2**	**Peak 3**	**Peak 4**	**peak 5**
$CoSe_2$-$FeSe_2$@GA	0.94	0.93	0.91		
$CoSe_2$-ZnSe@GA	0.96	0.91	0.96	0.94	
$CoSe_2$-$NiSe_2$@GA	1.00	0.98	0.99	0.99	0.98
$CoSe_2$	0.95	0.86	0.90		

Table S5. The calculated diffusion coefficients of $CoSe_2$-$FeSe_2$@GA, $CoSe_2$-ZnSe@GA and $CoSe_2$-$NiSe_2$.

Samples	$D_{DisCharge}$ ($cm^2/s \times 10^{-9}$)	D_{Charge} ($cm^2/s \times 10^{-9}$)
$CoSe_2$-$FeSe_2$@GA	20.683	15.550
$CoSe_2$-ZnSe@GA	7.416	6.752
$CoSe_2$-$NiSe_2$@GA	6.095	4.569

Calculation of the relative contents of $CoSe_2$, $FeSe_2$ and carbon in $CoSe_2$-$FeSe_2$@GA

As shown in **Figure 2d**, $CoSe_2$-$FeSe_2$@GA has a weight loss of 70.9wt%. The weight loss of the composite is mainly composed of three parts: the change of weight loss from $CoSe_2$ to Co_3O_4, the change of weight loss from $FeSe_2$ to Fe_2O_3 and the loss of carbon oxidation. W represents the weight percentage of $FeSe_2$. Since the ratio of cobalt to iron in the raw material is controlled at 1:1 and the molecular weight of $FeSe_2$ is similar with $CoSe_2$, the weight percentage of $CoSe_2$ is also W and the weight percentage of carbon is (100%-2W). Thus, according to the reaction equation (1)(2), the weight loss from pure $CoSe_2$ to Co_3O_4 is 63.0wt% and from pure $FeSe_2$ to Fe_2O_3 is 62.6wt%.

$3CoSe_2 + 8O_2 \rightarrow Co_3O_4 + 6SeO_2\uparrow$ (1)

$4FeSe_2 + 11O_2 \rightarrow 2Fe_2O_3 + 8SeO_2\uparrow$ (2)

$W \times 63.0\% + W \times 62.6\% + 100\% - 2W = 70.9\%$ (3)

Therefore, according to formula (3), it can be calculated that the content of $CoSe_2$, $FeSe_2$, and carbon in $CoSe_2$-$FeSe_2$@GA is 39.1wt%, 39.1wt%, and 21.8wt%.

Calculation of the relative contents of $CoSe_2$, ZnSe and Carbon in $CoSe_2$-ZnSe@GA

As shown in Figure 2d, $CoSe_2$-ZnSe@GA has a weight loss of 66.6wt%. The weight loss of the composite is mainly composed of three parts: the weight loss of $CoSe_2$ to Co_3O_4, the weight loss of ZnSe to ZnO and the weight loss of carbon oxidation. W represents the weight percentage of $CoSe_2$. Since the ratio of cobalt to zinc in the raw material is controlled at 1:1, the weight percentage of ZnSe is W and the weight percentage of carbon is (100%-2W). Thus, according to reaction equation (4), the weight loss from pure ZnSe to ZnO is 43.6wt%.

$2ZnSe + 3O_2 \rightarrow 2ZnO + 2SeO_2\uparrow$ (4)

$W \times 63.0\% + W \times 43.6\% + 100\% - 2W = 66.6\%$ (5)

Therefore, according to formula (5), it can be calculated that the content of $CoSe_2$, ZnSe and carbon in $CoSe_2$-ZnSe@GA is 35.8wt%, 35.8wt% and 28.4wt%

Calculation of the relative contents of $CoSe_2$, $NiSe_2$ and carbon in $CoSe_2$-$NiSe_2$@GA

As shown in Figure 2d, $CoSe_2$-$NiSe_2$@GA The weight loss is 70.1wt%. The weight loss of composite materials mainly consists of three parts: weight loss from $CoSe_2$ to Co_3O_4, weight loss from $NiSe_2$ to Ni_2O_3, and weight loss from carbon oxidation. W represents the weight percentage of $CoSe_2$, and since the cobalt nickel ratio in the raw material is controlled at 1:1.5, the weight percentage of carbon is (100% -2.5 W). Therefore, according to reaction equation (6), the weight loss from pure $NiSe_2$ to Ni_2O_3 is 40.0wt%.

$4NiSe + 7O_2 \rightarrow 2Ni_2O_3 + 4SeO_2\uparrow$ (6)

$W \times 63.0\% + 1.5W \times 40.0\% + 100\% - 2.5W = 70.1\%$ (7)

Therefore, according to formula (7), it can be calculated that the content of $CoSe_2$ and $NiSe_2$ in $CoSe_2$-$NiSe_2$@GA is 23.5wt%, 35.3wt% and the content of carbon is 41.2wt%.

References:

[1] Z. N. Cao, J. W. Cui, D. B. Yu, Y. Wang, J. Q. Liu, J. C. Zhang, J. Yan, Y. Zhang, S. H. Sun, Y. C. Wu, Synergistic engineering of architecture and composition in bimetallic selenide@carbon hybrid nanotubes for enhanced lithium- and sodium-ion batteries, *Adv. Funct. Mater.*, 2023, **33**, 2306862.

[2] H. Y. Zhu, Z. Y. Li, F. Xu, Z. X. Qin, R. Sun, C. H. Wang, S. J. Lu, Y. F. Zhang, H. S. Fan, Ni_3Se_4@$CoSe_2$ hetero-nanocrystals encapsulated into CNT-porous carboninterpenetrating frameworks for high-performance sodium-ion battery, *J. Colloid Interface Sci.*, 2022, **611**, 718-725.

[3] Z. Zhang, Y. Huang, X. D. Liu, X. Wang, P. B. Liu, Core−shell Co, Zn bimetallic selenide embedded nitrogen-doped carbon polyhedral frameworks assist in sodium-ion battery ultralong cycle, *ACS Sustainable Chem. Eng.*, 2020, **8,** 8381−8390.

[4] J. H. Li, Y. Y. He, Y. X. Dai, H. Z. Zhang, Y. X. Zhang, S. N. Gu, X. Wang, T. T. Gao, G. W. Zhou, L. Q. Xu, Heterostructure interface construction of cobalt/molybdenum selenides toward ultra-stable sodium-ion half/full batteries, *Adv. Funct. Mater.*, 2024, 2406915.

[5] Q. Zhang, M. L. Chen, J. Wang, C. F. Zhao, F. H. Cao, H. Li, H. P. Cong, C. L. Zhang, Ultrafine ZnSe/CoSe nanodots encapsulated in core–shell MOF-derived hierarchically porous N-doped carbon nanotubes for superior lithium/sodium storage, *J. Mater. Chem. A*, 2023, **11**, 5056.

[6] H. Shan, J. Qin, Y. C. Ding, H. M. K. Sari, X. X. Song, W. Liu, Y. C. Hao, J. J. Wang, C. Xie, J. J. Zhang, X. F. Li, Controllable heterojunctions with a semicoherent phase boundary boosting the potassium storage of $CoSe_2$/$FeSe_2$, *Adv. Mater.*, 2021, **33**, 2102471.

[7] B. W. Cong, X. R. Li, Y. H. Suo, G. Chen, Metal-organic framework derived bimetallic selenide embedded in nitrogen-doped carbon hierarchical nanosphere for highly reversible sodium-ion storage, *J. Colloid Interface Sci.,* 2023, **635**, 370 -378.

[8] L. Y. Zhang, B. C. Zhu, D. F. Xu, Z. B. Qian, P. Xie, T. Liu, J. G. Yu, Yolk-shell $FeSe_2$@$CoSe_2$/$FeSe_2$ heterojunction as anode materials for sodium-ion batteries with high rate capability and stability, *J. Mater. Sci. Technol.*, 2024, **172**, 185-195.

[9] N. Kitchamsetti, J. S. Cho, C. S. Chakra, Prussian blue analogue derived porous hollow nanocages comprising polydopamine-derived N-doped C coated $CoSe_2$/$FeSe_2$ nanoparticles composited with N-doped graphitic C as an anode for high-rate Na-ion batteries, *Chem. Eng. J.*, 2024, **495**, 153353.

[10] H. Tian, Z. Z. Xu, K. Liu, D. Wang, L. L. Ren, Y. M. Wei, L. Z. Chen, Y. Y. Chen, S. H. Liu, H. X. Yang, Heterogeneous bimetallic selenides encapsulated within graphene aerogel as advanced anodes for sodium-ion batteries, *J. Colloid Interface Sci.*, 2024, **670**, 152-162.

[11] L. Gao, Y. N. Ma, C. K. Zhang, M. L. Cao, Constructing heterostructured $CoSe_2$-SnSe nanoparticles incorporated carbon nanofibers for robust sodium storage, *Chem. Eng. Sci.*, 2024, **283**, 119390.